Mass-selected photodissociation studies of $AlPb_n^+$ clusters ($n = 7$–16): Evidence for the extraordinary stability of $AlPb_{10}^+$ and $AlPb_{12}^+$

Soumen Bhattacharyya,[1,*] Thanh Tung Nguyen,[1] Jorg De Haeck,[1] Klavs Hansen,[2] Peter Lievens,[1] and Ewald Janssens[1,†]

[1]*Laboratory of Solid-State Physics and Magnetism, KU Leuven, B-3001 Leuven, Belgium*

[2]*Department of Physics, University of Gothenburg, 41296 Gothenburg, Sweden*

(Received 19 June 2012; revised manuscript received 9 October 2012; published 5 February 2013)

We report fragmentation pathways and dissociation energies of $AlPb_n^+$ ($n = 7$–16) clusters. The clusters are produced with pulsed laser vaporization and studied in a supersonic molecular beam setup. They are mass selected and photodissociated with 532 and 355 nm laser light. Photofragments are thereafter mass separated in a tandem reflectron time-of-flight mass spectrometer. Bare Pb_n^+ ($n = 8$–16) clusters preferentially evaporate Pb atoms, with the exception of Pb_{15}^+ that fragments by loss of a Pb_2 dimer to form the stable Pb_{13}^+ cluster. The smallest $AlPb_n^+$ ($n = 7$–11) clusters also show mainly atomic Pb evaporation, whereas the favored fragmentation pathway of the larger clusters ($n = 12$–16) involves Pb_2 and Pb_3 fragments. $AlPb_{10}^+$ and $AlPb_{12}^+$ are the most intense fragments of several larger cluster sizes, demonstrating the high stability of these two sizes. Dissociation energies corresponding to the most facile fragmentation channel of $AlPb_n^+$ ($n = 11$–15) are bracketed from the measured laser fluence dependencies of the fragment intensities using constraints imposed by unimolecular reaction rates.

DOI: 10.1103/PhysRevB.87.054103 PACS number(s): 36.40.Qv, 36.40.Wa, 33.15.Ta

I. INTRODUCTION

A long-term goal of cluster science research is to synthesize chemically inert, particularly stable cluster species with specific properties that can be used as advanced material in nanotechnology applications.[1] Bimetallic clusters could be the building blocks of these advanced materials, since their physical and chemical properties can be engineered by manipulating size, shape, and composition.[2] However, apart from a few fullerenes[3] and endohedral fullerenes, only the Zintl ions have been isolated in macroscopic amounts and have been crystallized in well ordered lattices.[4] Among the variety of atomic clusters studied, group 14 clusters, especially pure and doped silicon clusters, have been investigated extensively, in part due to their importance in electronic devices. Computational studies have predicted a large number of highly symmetric icosahedral structures for heavier group 14 congeners.[5] The stability of several of these systems has been demonstrated by their high abundance in mass spectrometric studies on MS_n (M = Cr, Mn, Cu, Zn, and S = Si, Ge, Sn, Pb).[6] A few years ago, some of us reported the mass spectrometric discovery of the extremely stable $AlPb_{10}^+$ and $AlPb_{12}^+$ clusters.[7] Their high stability was attributed to their closed-packed structure and optimally filled electron shells. Following this, Chen *et al.*[8,9] calculated, using density functional theory (DFT), the electronic structures and stabilities of $Pb_{12}M^+$ clusters, where M represents group 13 elements such as B, Al, Ga, In, and Tl. They suggested that the high stabilities arise from the closed-shell nature of the subsystems, which are subject to the $2(N_\pi + 1)^2$ rule with $N_\pi = 1$. These suggestions are in line with the general principles for designing stable symmetrical clusters taking into account both electron shell closure rules and geometric arguments to form close-packed endohedral structures.[10] Rajesh *et al.* later investigated Pb_nM (M = C, Al, In, Mg, Sr, Ba, and Pb; $n = 8$, 10, 12, and 14) theoretically,[11,12] and Bai *et al.* found that $FePb_{12}$ has a stable icosahedral structure.[13] Schäfer *et al.* probed the position of a Mg atom in lead clusters by electric deflection studies and reported the formation of endohedral Mg doped lead cage structures.[14] Also the composition dependence of the electrical dipole moments of Sn_mPb_n ($7 \leqslant n + m \leqslant 15$) nanoalloys has been discussed.[15] Recently the onset of cluster assembling was studied via the formation of cluster dimers, $[MPb_{10}]_2$ (M = Fe, Co, Ni), built up of MPb_{10} endohedral square antiprisms.[16] Theoretical as well as photoelectron spectroscopic investigations have shown that the anionic clusters Pb_{10}^{2-}, Pb_{12}^{2-}, and also Sn_{12}^{2-} are highly aromatic and have caged structures.[8,17–20] Also the role of cage aromaticity for larger doped group 14 clusters has been studied.[21,22] It is also worth noting that the ligand-free bimetallic clusters, $M@Pb_{12}^{2-}$ and $M@Pb_{10}^{2-}$ with M = Ni, Pd, Pt, could be synthesized in solution.[4]

The stability of a cluster can be investigated using photofragmentation. Clusters are intrinsically stable and some excess energy, provided by, e.g., photoexcitation, is needed to induce fragmentation. Statistical models can then be used, in combination with recorded fragmentation yields, to extract dissociation energies. This approach has been followed by several groups to study the stability of size selected clusters.[23–31]

In this work, we present a mass-selective photodissociation study of pure Pb_n^+ ($n = 8$–16) and aluminum doped $AlPb_n^+$ ($n = 7$–16) clusters using 532 and 355 nm laser light. Conclusive evidence for the extraordinary high stability of $AlPb_{10}^+$ and $AlPb_{12}^+$ is given. Fragmentation pathways combined with mass spectrometric results allow commenting on structural characteristics of these species. In addition, laser fluence dependent studies on $AlPb_n^+$ ($n = 11$–15) enabled us to set limits on the dissociation energies corresponding to their most facile fragmentation channels.

II. EXPERIMENT

Bimetallic $AlPb_n^+$ cluster cations are produced in a pulsed dual-target dual-laser vaporization source[32] coupled to a newly built dual reflectron high-resolution ($m/\Delta m \sim 10\,000$) time-of-flight mass spectrometer (RTOF), which uses curved field extraction optics.[33] However, the mass resolution achieved in this study is around 4000 due to the use of simple two-plate

extraction optics to increase the signal intensity. In the cluster source rectangular aluminum and lead targets are ablated by two independent pulsed Nd-YAG lasers at 532 nm having energy density ~8 mJ/cm^2. Following vaporization, helium gas is introduced into the source to initiate cluster formation. Supersonic expansion into the high vacuum through a nozzle generates a molecular beam with clusters. We assume that the temperature of the clusters equals the temperature of the cluster source (i.e., 300 K). Heat exchange with the walls of the source occurs via the He carrier gas. The validity of this assumption was confirmed in earlier work where argon absorption was studied as function of the source temperature.[34,35]

Doped lead clusters are skimmed into the extraction chamber and cationic clusters are accelerated perpendicularly into the RTOF through extraction optics. The cationic Pb_n^+ or $AlPb_n^+$ clusters of interest are mass selected at the temporal focal point of the first reflectron by a wire type mass gate.[36,37] These mass selected clusters are then exposed to the second (532 nm) or third (355 nm) harmonics of a Q-switched Nd-YAG laser close to the mass gate, and the resulting photofragments are mass separated by the second reflectron before hitting a chevron type MCP detector.

III. RESULTS AND DISCUSSION

A. Photofragmentation channels

The photodissociation of $AlPb_n^+$ (n = 7–16) was studied with 355 nm light as a function of laser fluence in the 5–80 mJ/cm^2 range with a slightly defocused laser beam of diameter 13 mm. However, for n = 7–10 and n = 16, photofragments were only observed for fluences above 60 mJ/cm^2. For these sizes the low intensity of the photofragments did not allow us to perform a fluence dependence study. The dissociation channels of $AlPb_n^+$ (n = 7–16) with 355 nm light are given in Table I. For the smallest $AlPb_n^+$ (n = 7–9) clusters only one dissociation channel is observed, which consists of monomer Pb atom evaporation. The larger $AlPb_n^+$ clusters (n = 10,11,13,16) also decay through one dissociation channel only, as evidenced by the lower laser fluence spectra. However, at higher fluence (around 30 mJ/cm^2) a second fragment appears with the fragment seen at lower fluence remaining more intense. This second fragment results from the absorption of two (or more) photons, which is concluded from the increase of the ratio of the intensities of second to primary fragments with laser fluence as well as its appearance at higher fluence only. $AlPb_{12}^+$ appears to be an exception; here we find two parallel dissociation channels, i.e., monomer and dimer decay, with the dimer evaporation channel being the most intense. Both fragments originate directly from the parent cluster, because the ratio of the fragment peak intensities does not (for low laser fluence) depend on the laser fluence. The sequential and parallel fragmentation paths observed for $AlPb_n^+$ ($n \geqslant 10$) are included in Table I.

TABLE I. Dissociation channels for $AlPb_n^+$ (n = 7–16). The primary fragment is the parent cluster in the sequential dissociation process.

Parent cluster	Primary dissociation channel	Sequential†/parallel‡ dissociation
$AlPb_7^+$	$AlPb_6^+ + Pb$	
$AlPb_8^+$	$AlPb_7^+ + Pb$	
$AlPb_9^+$	$AlPb_8^+ + Pb$	
$AlPb_{10}^+$	$AlPb_9^+ + Pb$	$AlPb_8^+ + Pb$†
$AlPb_{11}^+$	$AlPb_{10}^+ + Pb$	$AlPb_9^+ + Pb$†
$AlPb_{12}^+$	$AlPb_{10}^+ + Pb_2$	$AlPb_{11}^+ + Pb$‡
$AlPb_{13}^+$	$AlPb_{12}^+ + Pb$	$AlPb_{10}^+ + Pb_2$†
$AlPb_{14}^+$	$AlPb_{12}^+ + Pb_2$	
$AlPb_{15}^+$	$AlPb_{12}^+ + Pb_3$	
$AlPb_{16}^+$	$AlPb_{14}^+ + Pb_2$	$AlPb_{12}^+ + Pb_2$†

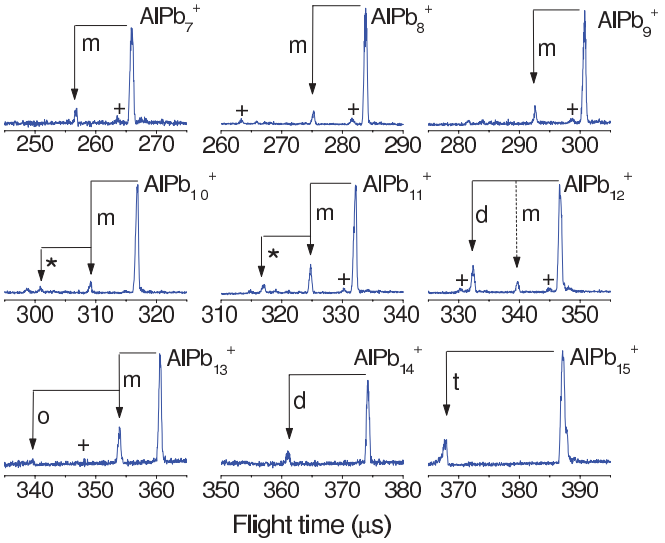

FIG. 1. (Color online) Fragmentation of $AlPb_n^+$ (n = 7–15) with 70 mJ/cm^2 laser light (355 nm). The dissociation channels (from parent to daughter) are indicated by arrows. Arrows labeled with m, d, and t correspond to neutral Pb, Pb_2, and Pb_3 loss respectively. The dashed arrow for $AlPb_{12}^+$ indicates a parallel monomer evaporation channel. $*$ and o correspond to sequential neutral Pb and Pb_2 evaporation from the first generation fragments. Additional peaks marked with "+" correspond to Pb_n^+ and $AlPb_{n-1}^+$ clusters that are transmitted due to the limited resolution of the mass selector.

$AlPb_n^+$ (n = 10, 11, and 13) clusters are found to dissociate via monomer evaporation, whereas $AlPb_n^+$ (n = 12, 14, and 16) fragments via Pb_2 loss to form $AlPb_{n-2}^+$ daughter ions, and $AlPb_{15}^+$ dissociates by Pb_3 emission to form the stable $AlPb_{12}^+$ daughter ion. Figure 1 shows mass spectra recorded after photodissociation of mass selected $AlPb_n^+$ (n = 7–15) clusters with 355 nm laser light at a fluence of 70 mJ/cm^2. For all sizes, 532 nm laser light yielded the same primary dissociation channels as the 355 nm laser light, but no sequential dissociation channels are observed (not shown on figure). Only $AlPb_{12}^+$ could not be fragmented with the 532 nm laser light, most likely because of energy reasons. An alternative explanation could be that the photoabsorption cross section is effectively zero.

The fragmentation channels recorded for $AlPb_n^+$ (n = 12–16) show larger fragments, contrasting with the observations for bare Pb_n^+ clusters that all, except Pb_{15}^+, fragment by monomer evaporation. Mass spectra recorded after

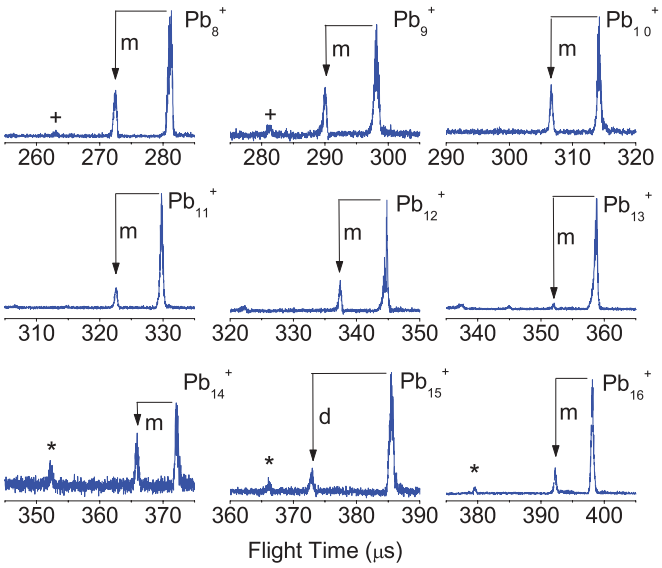

FIG. 2. (Color online) Fragmentation of Pb_n^+ (n = 8–16) with 100 mJ/cm^2 laser light (355 nm). The dissociation channels (from parent to daughter) are indicated by arrows labeled with m and d for neutral Pb and Pb_2 loss, respectively. Peaks labeled with $*$ correspond to Pb_{n-3}^+ fragments. These could be direct fragments from the corresponding Pb_n^+ parents or sequential fragments from Pb_{n-1}^+. Additional peaks marked with "+" correspond to Pb_{n-1}^+ clusters that are transmitted due to the limited resolution of the mass selector.

photodissociation of size selected pure Pb_n^+ (n = 8–16) with 100 mJ/cm^2 of 355 nm laser light are given in Fig. 2. The pure lead cluster cations all decay by monomer evaporation, except Pb_{15}^+ which decays by dimer evaporation to form the stable Pb_{13}^+ daughter cluster. The most facile fragmentation channels of cationic lead clusters have been computed by Rajesh and Majumder from total energies of the lowest energy isomers found in a DFT study at the generalized gradient approximation (GGA) level including spin-orbit coupling effects.[38] Their predictions are in excellent agreement with the current results: monomer decay is the preferred channel for all Pb_n^+ clusters (n = 2–14) with the exception of Pb_{15}^+. Pb_{15}^+ decays by Pb_2 loss, confirming the higher stability of Pb_{13}^+, which is predicted to have a slightly distorted icosahedral symmetry. In addition the predicted fragmentation energies are all below 2.7 eV, which implies that a single 355 nm photon can induce photodissociation provided that the kinetic shift is not excessively large.[38]

The observation of Pb_2 fragments from $AlPb_n^+$ (n = 12 and 14) to form more stable $AlPb_{n-2}^+$ and the Pb_3 fragment from $AlPb_{15}^+$ leading to $AlPb_{12}^+$ is of particular interest as most metallic clusters show atom evaporation only. Dimer evaporation has previously been observed in alkali metal and coinage metal clusters: lithium, sodium, copper, silver, gold, and doped gold clusters.[25,30,31,37,39,40] In these cases, the enhanced dimer evaporation channel is correlated strongly with an enhanced stability of the daughter cluster, reflecting either a closed electronic shell structure or a strong odd-even amplitude.

As seen from Table I, $AlPb_{10}^+$ and $AlPb_{12}^+$ appear as products in the photon induced decay chain of most studied $AlPb_n^+$ ($n > 10$) clusters. $AlPb_{10}^+$ is formed as primary fragment from $AlPb_{11}^+$ and $AlPb_{12}^+$ and as a secondary fragment from the photodissociation of the $AlPb_{13}^+$ parent. Likewise, $AlPb_{12}^+$ is formed as a primary photodissociation fragment from $AlPb_n^+$ (n = 13–15) and in the sequential decay process from $AlPb_{16}^+$.

The photon induced unimolecular dissociation tends to terminate at fragment ions with enhanced stabilities,[41] and, if certain clusters are formed as main fragment for several initial cluster sizes, they can be identified as relatively stable units. Our earlier mass spectrometric observations already indicated an extraordinary stability of $AlPb_{10}^+$ and $AlPb_{12}^+$.[7] However, a high abundance of a specific size in a mass spectrum does not always reflect a higher stability, because cluster formation in a laser ablation source is sensitive to production parameters, and it is not obvious that the conditions for application of the evaporative ensemble theory are fulfilled.[41] Furthermore, the presence of the dimer channel seriously complicates the analysis. In the present investigation, wherein clusters are first mass selected, stability information is extracted from the intensity ratio of daughter to parent signals after laser irradiation and not from the intensity of the clusters as produced in the source. The results prove that the $AlPb_{10}^+$ and $AlPb_{12}^+$ clusters are significantly more stable than their precursors in the decay chain.

B. Likely geometric structures

The structures of the two magic sizes $AlPb_{10}^+$ and $AlPb_{12}^+$ have been described by a highly symmetric bicapped-square-antiprism with D_{4d} symmetry and by a perfect icosahedron with I_h symmetry and the Al atom encapsulated at the center, respectively.[7–9] Calculations for $AlPb_n^+$ clusters (n = 1–12) predict that the Al atom is located in a Pb_n cage from size n = 9 onwards.[9,10]

The mass spectrometric results and photofragmentation channels provide indirect qualitative information about the structure of the clusters. While we could produce pure Al_n^+ and Pb_n^+ cationic clusters with n = 1–25, we could only produce doped $AlPb_n^+$ clusters in the size range n = 6–17. Also, in our previous mass spectrometric investigations n = 6 was the smallest size for which doped clusters could be produced.[7] It is also observed that, while single Al-doped $AlPb_n^+$ clusters are produced in high abundance, the intensity of pure Pb_n^+ clusters is significantly smaller than the intensities that are obtained without simultaneous ablation of the aluminum target. In the current experiment we never observed loss of the dopant Al atom. It should, however, be noted that it was not possible to establish the dissociation channels for $AlPb_6^+$ because of its low intensity. Since a minimum of six Pb atoms are required to bind an Al atom and we did not see evaporation of atomic Al, it is tempting to imagine a geometric structure of the cluster with the Al atom endohedrally encapsulated into the Pb_n cage. A similar conclusion was drawn by Schäfer *et al.* for $MgPb_n^+$ clusters, where a minimum of ten Pb atoms are required to pick up one Mg atom.[14] However, conclusions about the structure based on observed unimolecular branching ratios are inherently inconsistent because branching ratios are determined by the stability of the products and not by the ground-state structure of the parent, and our conclusions concerning the structure are therefore only tentative.

TABLE II. Ionization energies (IEs) of $AlPb_n$ (n = 6–14). Calculated IE values are from Ref. 8.

	IE (eV)	
Cluster	This work	Calculated
$AlPb_6^+$	<7.4	6.6
$AlPb_7^+$	<7.4	6.2
$AlPb_8^+$	<7.4	6.0
$AlPb_9^+$	<7.4	5.5
$AlPb_{10}^+$	<6.2	5.1
$AlPb_{11}^+$	<7.4	5.5
$AlPb_{12}^+$	<5.8	4.3
$AlPb_{14}^+$	<6.2	

C. Ionization energies

If the dissociation takes place on the ground-state potential energy surface, the charge of the parent cation cluster will reside on the fragment species with the lowest ionization potential. The observation that the primary fragmentation channel is found to be wavelength (532 and 355 nm) independent for all sizes supports this claim. This idea in combination with the measured ionization energies (IEs) of bare Pb_n clusters (n = 1–7) by electron impact (Pb: 7.4 eV; Pb_2: 6.2 eV; Pb_3: 5.8 eV; Pb_4: 5.7 eV),[42] allows us to comment on the IEs of $AlPb_n$. The cationic $AlPb_n^+$ clusters (n = 6–9, 11) are produced from their respective parents via loss of one Pb atom. Since the charge is retained on the doped clusters, the IEs of the neutral $AlPb_n$ (n = 6–9, 11) must be less than that of the Pb atom (7.4 eV). Similarly, $AlPb_n^+$ (n = 10 and 14) are produced via Pb_2 loss from $AlPb_{n+2}^+$, so the IEs of $AlPb_{10}$ and $AlPb_{14}$ must be less than that of Pb_2 (6.2 eV). The IE of $AlPb_{12}$ is less than 5.8 eV (IE of Pb_3) since it is produced from the $AlPb_{15}^+$ parent cluster via neutral Pb_3 loss. An overview of the bracketed IEs of neutral $AlPb_n$ is given in Table II along with their theoretical values from calculations at the B3LYP level of theory.[9] It can be seen that the bracketed IEs are consistent with the theoretical values.

D. Dissociation energies

In order to extract dissociation energies, $D_{n,\Delta n}$, of an n-atom cluster dissociating into $n-\Delta n$ and Δn atom fragments from the experimentally relevant evaporative rate constant $k_n(E)$, an expression connecting these two via the excitation energy (E) is needed. According to the detailed balance theory, the measured rate constants can be approximated as[31,37,43–46]

$$k_{n,\Delta n}(E) \cong \omega_{n,\Delta n}\frac{\rho_{n-\Delta n}(E-D_{n,\Delta n})}{\rho_n(E)}, \quad (1)$$

where ρ_n and $\rho_{n-\Delta n}$ are the parent and daughter level densities. The frequency factor $\omega_{n,\Delta n}$ depends on the cluster size as well as on the dissociation channel. The level densities are calculated using the high-energy limit of harmonic oscillators:[31]

$$\rho_n(E) = \frac{[E+(3n-6)\hbar\omega_D/2]^{3n-7}}{(3n-7)!(\hbar\omega_D)^{3n-6}}, \quad (2)$$

where ω_D is the Debye frequency of Pb ($\omega_D\hbar/k_B$ = 88 K).[47] For monomer evaporation, $\Delta n = 1$, the frequency factor is given by[31]

$$\omega_{n,1} = \frac{8\pi g\mu\sigma_{n-1}}{h^3}(k_BT_d)^2, \quad (3)$$

where $g = 2$ is the electronic degeneracy of a free Pb atom, μ is the reduced mass of the dissociation channel, σ_{n-1} is the geometric cross section of capture of an atom ($\sigma_{n-1} = \pi r^2[(n-1)^{1/3}+1]^2$ with r = 1.46 Å the covalent radius of Pb), and T_d is the daughter temperature. The derived dissociation energies will not be very sensitive to the temperature and we will summarily use the value k_BT_d = 0.05 eV for the daughter temperature.[48] The dissociation energy for monomer evaporation, $D_{n,1}$, then follows from Eqs. (1)–(3) as

$$D_{n,1} = E+(3n-9)\hbar\omega_D/2 - [E+(3n-6)\hbar\omega_D/2]\left(\frac{k_{n,1}(E)}{\omega'_{n,1}}\right)^{1/3n-7} \quad (4)$$

with $\omega'_{n,1} = \omega_{n,1}(\hbar\omega_D/k_BT_d)^3$, which is of the order 10^{15}–10^{16} s^{-1} (e.g., $\omega'_{n,1} = 8.1\times10^{15}$ s^{-1} for $AlPb_{11}^+$). The excitation energy of the cluster is $E = E_{th}+h\nu$, where E_{th} is the thermal energy and $h\nu$ is the excitation energy resulting from the absorption of a photon. $E_{th} = (k_BT-\hbar\omega_D/2)(3n-6)$ given by the leading order term in the heat capacity above the Debye temperature of the n-atom cluster.

The mass spectrometric observations are used to derive the evaporative rate constant $k_n(E)$. The width of the energy distribution prior to laser excitation is given by $2\sqrt{C/k_B}k_BT = 2\sqrt{3n-6}k_BT$. The largest value, for $AlPb_{16}^+$, corresponds to 0.23 eV or only 0.054 times the total energy after absorption of a 355 nm photon. This worst case corresponds to a range of rate constants of about a factor of exp(1), which is the limit of validity of approximating the thermal distribution of rate constants with a single value. For smaller clusters, the approximation is better and we proceed with using a single value to describe the decay.

When the laser fluence is in the single photon absorption regime, immediately after the laser fires (t = 0), there are basically two types of clusters: those that did absorb one single photon and those that did not absorb any photon: $I(0) = I^*(0)+I^0(0)$ with I^* and I^0 the intensity of the clusters that absorbed one and zero photons, respectively. The two fractions are given by

$$I^*(0) = \left(\frac{\sigma F_L}{h\nu}\right)I(0), \quad I^0(0) = \left(1-\frac{\sigma F_L}{h\nu}\right)I(0), \quad (5)$$

where σ is the photon absorption cross section, F_L is the laser fluence, and $h\nu$ the photon energy. In addition, one has to account for the fraction of clusters that are exposed to the laser beam. This imperfect overlap factor between the ion packet and laser beam is estimated to be 75% based on geometry arguments (dimensions of the mass gate and the laser beam, and quality of temporal focus point for the mass selective fragmentation). The intensities of the cluster signal are corrected for this overlap. The dissociation energies derived at the end of the analysis are not very sensitive to the overlap factor. A change by 10% results in a change of $D_{n,\Delta n}$ by a few percent only. Clusters that absorbed a photon (with an energy larger than the dissociation energy) will be subject to

unimolecular dissociation at rate $k_n(E)$, while the intensity of the nonexcited clusters is constant. The ratio between the numbers of non-decayed and initial clusters is then

$$\frac{I(t)}{I(0)} = 1 - \frac{\sigma F_L}{h\nu}(1 - e^{-k_n(E)t}), \tag{6}$$

with $I(t)$ being the number of parent clusters at the time t given that the dissociation laser fires at $t = 0$ and the clusters reach the second reflectron at time t.

From the geometry of the instrument and the kinetic energies of the clusters, t can be estimated (e.g., $\sim$39 μs for $AlPb_{12}^+$). The parent intensity at $t = 0$, $I(0)$, can be approximated by the sum of the parent and the fragment ion intensities at t. If σ were known, $k_n(E)$ could be obtained from the intensities of the peaks in the mass spectra vs F_L using Eq. (6). Unfortunately σ cannot be determined directly. However, the fluence dependence data provide a range for σ. From Eq. (5) it is clear that in the single photon regime, $1 - \sigma F_L/h\nu$ and $\sigma F_L/h\nu$ are equal to the probabilities that none and one photon are absorbed by the cluster, respectively. The maximal laser fluence in the single-photon regime must be such that $\sigma F_L/h\nu$ is smaller than unity, providing an upper boundary for σ. The depletion of the parent peak at the maximal fluence (in the linear regime) provides a lower boundary for σ: $1 - I(t)/I(0) < \sigma F_L/h\nu$ since at least one photon is to be absorbed to trigger dissociation. Following this reasoning we obtain, depending on the cluster size, typical ranges of 0.01–0.08 Å^2 for the absorption of a 2.33 eV photon and of 0.03–0.15 Å^2 for the absorption of a 3.55 eV photon.

Figure 3 shows the variation of the intensity ratio of primary and secondary fragments to the parent signal as a function of the dissociation laser fluence. The fluence curves measured

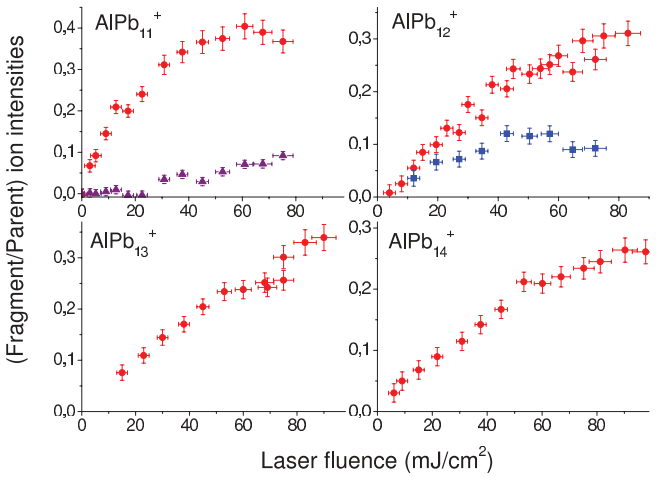

FIG. 3. (Color online) Laser fluence dependence for the (a) $AlPb_{11}^+ \rightarrow AlPb_{10}^+ \rightarrow AlPb_9^+$ and (b) $AlPb_{12}^+ \rightarrow AlPb_{10}^+$ and $AlPb_{12}^+ \rightarrow AlPb_{11}^+$ dissociation channels observed using 355 nm laser light, and (c) $AlPb_{13}^+ \rightarrow AlPb_{12}^+$ and (d) $AlPb_{14}^+ \rightarrow AlPb_{12}^+$ dissociation channels as seen with 532 nm laser light. Circles and triangles represent primary and secondary daughter ions intensities, respectively. The squares for $AlPb_{12}^+$ correspond to the parallel monomer dissociation channel. The error bars represent uncertainties related to laser power fluctuations and the determination of the ion intensities (baseline dependence, fluctuations of the cluster source condition, etc.).

for $AlPb_n^+$ (n = 11–15) at either 355 nm or 532 nm laser wavelengths all show a linear dependence below a certain threshold fluence, which indicates a single-photon process, with the possible exception of $n = 11$. In the Appendix we discuss quantitatively the possibility that greatly differing cross sections can give rise to a multiphoton process with a fluence dependence similar to a true one-photon process. It is shown that this is not a possibility.

Given the boundaries for σ, an upper and lower value for $k_n(E)$ and thus for $D_{n,\Delta n}$ can be derived. However, if $k_n(E)t \gg 1$ most excited clusters are dissociated on the time scale of the experiment. Since high rate constants correspond to low $D_{n,\Delta n}$ values, for most sizes only an upper boundary for $D_{n,\Delta}$ could be derived. The dissociation energies for clusters that decay by monomer evaporation, $AlPb_{11}^+$ and $AlPb_{13}^+$, are determined to be in the ranges $D_{11,1} \leqslant 2.04$ eV and $D_{13,1} = 1.80$–1.92 eV, respectively.

Equation (3) cannot be used if the fragmentation occurs by dimer or trimer evaporation. The frequency factor for dimer ($\Delta n = 2$) and trimer ($\Delta n = 3$) evaporation differs from that of a monomer because the rotational and vibrational degrees of freedom of the light fragment must be included in the level density. Applying a similar procedure as in Eq. (4) provides for the dimer decay:

$$D_{n,2} = E + (3n - 12)\hbar\omega_D/2 - [E + (3n - 6)\hbar\omega_D/2]\left(\frac{k_{n,2}(E)}{\omega_{n,2}}\right)^{1/3n-7} \tag{7}$$

with[37]

$$\omega_{n,2} = \omega'_{n,1} 0.809 \left(\frac{k_B T_d}{B_{\text{dimer}}}\right)\left(\frac{k_B T_d}{\hbar\omega_v}\right)\left(\frac{\hbar\omega_D}{0.05\text{ eV}}\right)^3 = 223\omega'_{n,1}. \tag{8}$$

The factor 0.809 is the symmetry number for the Pb_2 dimer considering the natural abundances of its four isotopes. In addition, there is a factor 2 from the reduced mass of the channel and a factor of 1/2 from the absence of electronic degeneracy of the atom. The rotational constant B_{dimer} is 0.018 8534 cm^{-1} and $\hbar\omega_v = 109.6$ cm^{-1}.[49] The dissociation energy ranges determined using Eq. (7) for dimer evaporation from $AlPb_{12}^+$ and $AlPb_{14}^+$ give $D_{12,2} = 2.33$–2.98 eV and $D_{14,2} \leqslant 2.07$ eV, respectively.

The frequency factor for trimer evaporation can be written as

$$\omega_{n,3} = \omega'_{n,1} 1.91 \left(\frac{k_B T_d}{B_{\text{dimer}}}\right)^{3/2}\left(\frac{k_B T_d}{\hbar\omega_v}\right)^3\left(\frac{\hbar\omega_D}{0.05\text{eV}}\right)^6 = 3.0 \times 10^3 \omega'_{n,1} \tag{9}$$

where it is assumed that the bond lengths in the trimer are equal to the dimer bond length (which explains the appearance of the dimer rotational constant in the equation) and with $\hbar\omega_v = 117$ cm^{-1}.[50] Following a similar procedure for the trimer emission from $AlPb_{15}^+$, it is found that $D_{15,3} \leqslant 2.09$ eV.

The derived ranges for the dissociation energies are summarized in Table III. These data show that (i) the dissociation energies of $AlPb_n^+$ (n = 11–15) vary strongly with cluster size. $AlPb_{12}^+$ is by far the most stable cluster of the investigated size range. (ii) A single 355 nm photon (3.49 eV) leads

TABLE III. Dissociation energies ($D_{n,\Delta}$) of the $AlPb_n^+$ (n = 11–15) clusters associated with the dissociation channels $AlPb_n^+ \rightarrow AlPb_{n-\Delta n}^+ + Pb_{\Delta n}$.

n,Δn	$D_{n,\Delta n}$ (eV)
11,1	$D_{11,1} \leqslant 2.04$
12,2	$2.33 \leqslant D_{12,2} \leqslant 2.98$
13,1	$1.80 \leqslant D_{13,1} \leqslant 1.92$
14,2	$D_{14,2} \leqslant 2.07$
15,3	$D_{15,3} \leqslant 2.09$

to photodissociation of all investigated clusters, while a single 532 nm photon (2.33 eV) cannot induce photofragmentation of $AlPb_{12}^+$, in line with the observation discussed in Sec. III A. (iii) The experimental dissociation energies for $AlPb_{11}^+$ ($D_{11,1} \leqslant 2.04$ eV) and $AlPb_{12}^+$ ($2.33 \leqslant D_{12,2} \leqslant 2.98$ eV) can be compared with calculated values of 2.98 and 3.75 eV, respectively (see supporting information of Ref. 10). Although the calculated values are significantly higher than the experimental ones, the change from $AlPb_{11}^+$ to $AlPb_{12}^+$ and the preferred fragmentation channel are consistent. Moreover, it was shown for pure lead clusters that calculated binding energies can be significantly overestimated (by up to 1 eV) if spin-orbit coupling is ignored in the total energy calculations.[38] The experimental dissociation energies are within an energy range that is comparable to the dissociation energy range predicted computationally, including the spin-orbit coupling effect, for bare Pb_n^+ (n=10–15) clusters (i.e., 1.8–2.7 eV with the exception of Pb_{14}^+ for which the monomer dissociation energy is predicted to be as low as 1.1 eV).[38]

IV. CONCLUSIONS

The fragmentation pathways of mass selected $AlPb_n^+$ (n = 7–16) clusters are investigated in photodissociation experiments using 532 and 355 nm laser light. $AlPb_{10}^+$ and $AlPb_{12}^+$ appear as the daughter fragments of all larger clusters, which conclusively proves the high stability of these two clusters. Ionization energies are bracketed and are in line with theoretical values. Analysis of the laser fluence dependence of the fragment intensities established that the primary fragments are produced from one photon absorption processes. The dissociation energies of the most facile fragmentation channel of $AlPb_n^+$ (n = 11–15) are bracketed based on the laser fluence dependence of the photon induced unimolecular decay. The dissociation energy of $AlPb_{12}^+$ is shown to be significantly higher than that of the neighboring cluster sizes.

ACKNOWLEDGMENTS

This work is supported by the Research Foundation–Flanders (FWO), the KU Leuven Research Council (BOF, GOA, and IDO programs), the Belgian Interuniversity Attraction Poles (IAP) research program, and the Department of Physics of the University of Gothenburg.

APPENDIX: PHOTON ABSORPTION STATISTICS

This Appendix calculates the distribution of photons absorbed when the first photon is absorbed with a much smaller cross section than the following. The calculation will be schematic: The first photon is absorbed with a cross section σ_0 and the following with the much larger cross section σ. This is intended to mimic the situation where the energy of the first absorbed photon equilibrates and heats the cluster, leading to an increase of the oscillator strength at the relevant photon energy relative to the cold cluster. The laser pulse is assumed to be square in time, with a duration t_0, and with intensity I so that the fluence F is given by It_0. We define $\lambda \equiv It_0\sigma$, corresponding to one less than the average total number of photons absorbed if the first is absorbed at the beginning of the pulse.

If a cluster absorbs the first photon at time t, the time left to absorb more photons is $t_0 - t$. During that time a Poisson distribution is created in the number of secondary photons, with mean value $\lambda(t_0 - t)/t_0$. We can therefore find the distribution of photons absorbed as the integral over Poisson distributions created at different times, multiplied with a source factor:

$$P_{n+1} = \int_0^{t_0} e^{-\lambda(1-t/t_0)} \frac{[\lambda(1-t/t_0)]^n}{n!} \left(-\frac{dP_0}{dt}\right) dt. \quad \text{(A1)}$$

Here $n \geqslant 0$. The $n+1$ appears on the left-hand side here instead of n to account for the initial photon absorption. The last bracket is the production rate of clusters having absorbed one photon and is equal to

$$-\frac{dP_0}{dt} = \sigma_0 I e^{-\sigma_0 It} = \frac{\sigma_0}{\sigma t_0}\lambda e^{-\lambda t\sigma_0/t_0\sigma}. \quad \text{(A2)}$$

With this and a substitution in the integral we have (for $n \geqslant 0$)

$$P_{n+1} = \frac{\sigma_0}{\sigma} e^{-\lambda\sigma_0/\sigma} (1-\sigma_0/\sigma)^{-n-1} \int_0^{\lambda(1-\sigma_0/\sigma)} e^{-y} \frac{y^n}{n!} dy, \quad \text{(A3)}$$

and for the zero photon abundance

$$P_0 = e^{-\lambda\frac{\sigma_0}{\sigma}}. \quad \text{(A4)}$$

The sum of probabilities over all n gives unity, as required.

The integrals can be calculated to give the P's in closed form. It will be sufficient here to calculate the expression for $n = 1$, which is

$$P_1 = \frac{\sigma_0}{\sigma} e^{-\lambda\sigma_0/\sigma} (1-\sigma_0/\sigma)^{-1} (1 - e^{-\lambda(1-\sigma_0/\sigma)}). \quad \text{(A5)}$$

For P_2 and P_3 we use the relation obtained by a single partial integration:

$$P_{n+1} = P_n - \frac{\sigma_0}{\sigma} e^{-\lambda} \left(1 - \frac{\sigma_0}{\sigma}\right)^{-1} \frac{\lambda^n}{n!}. \quad \text{(A6)}$$

This gives, with the definition $\lambda' \equiv \lambda(1-\sigma_0/\sigma) \approx \lambda$,

$$\frac{P_2}{P_1} = \frac{1 - e^{-\lambda'} - \lambda e^{-\lambda'}}{1 - e^{-\lambda'}},$$
$$\frac{P_3}{P_2} = \frac{1 - e^{-\lambda'} - \lambda e^{-\lambda'} - \lambda^2/2e^{-\lambda'}}{1 - e^{-\lambda'} - \lambda e^{-\lambda'}}. \quad \text{(A7)}$$

A numerical estimate of these two expressions between $\lambda = 0.01$ and 1 gives the result that the ratio P_3/P_2 is 0.67

times the ratio P_2/P_1 and is increasing with λ. Consequently, even for a very small degree of two-photon absorption, an almost equal amount of three-photon absorption will take place. Even for the smallest photon energy used in the present experiments, three-photon absorption can be expected to give rise to several fragmentation events. The conclusion is that the linear fluence dependences in the data must be due to single-photon absorption.

*On leave from Atomic & Molecular Physics Division, Bhabha Atomic Research Centre, Mumbai 400085, India.
†ewald.janssens@fys.kuleuven.be

[1] J. A. Alonso, *Structure and Properties of Atomic Nanoclusters* (Imperial College Press, London, 2005).
[2] R. Ferrando, J. Jellinek, and R. L. Johnston, Chem. Rev. **108**, 845 (2008).
[3] H. W. Kroto, J. R. Heath, S. C. Obrien, R. F. Curl, and R. E. Smalley, Nature (London) **318**, 162 (1985).
[4] E. N. Esenturk, J. Fettinger, and B. Eichhorn, J. Am. Chem. Soc. **128**, 9178 (2006).
[5] V. Kumar and Y. Kawazoe, Appl. Phys. Lett. **80**, 859 (2002).
[6] S. Neukermans, X. Wang, N. Veldemans, R. E. Silverans, and P. Lievens, Int. J. Mass. Spectrom. **252**, 145 (2006).
[7] S. Neukermans, E. Janssens, Z. F. Chen, R. E. Silverans, P. v. R. Schleyer, and P. Lievens, Phys. Rev. Lett. **92**, 163401 (2004).
[8] D. L. Chen, W. Q. Tian, W. C. Lu, and C. C. Sun, J. Chem. Phys. **124**, 154313 (2006).
[9] D. L. Chen, W. Q. Tian, and C. C. Sun, Phys. Rev. A **75**, 013201 (2007).
[10] Z. Chen, S. Neukermans, X. Wang, E. Janssens, Z. Zhou, R. E. Silverans, R. B. King, P. v. R. Schleyer, and P. Lievens, J. Am. Chem. Soc. **128**, 12829 (2006).
[11] C. Rajesh and C. Majumder, Chem. Phys. Lett. **430**, 101 (2006).
[12] C. Rajesh and C. Majumder, J. Chem. Phys. **128**, 024308 (2008).
[13] Y. J. Bai, H. Y. Cheng, H. Q. Sun, N. Xu, and K. M. Deng, Physica B **406**, 3781 (2011).
[14] S. Schäfer and R. Schäfer, ChemPhysChem **9**, 1925 (2008).
[15] S. Heiles, S. Schäfer, and R. Schäfer, Phys. Chem. Chem. Phys. **12**, 247 (2010).
[16] X. Chen, K. Deng, C. Xiao, J. Chen, and D. E. Ellis, Comput. Theor. Chem. **971**, 73 (2011).
[17] P. v. R. Schleyer and H. Jiao, Pure Appl. Chem. **68**, 209 (1996).
[18] D. L. Chen, W. Q. Tian, J. K. Feng, and C. C Sun, J. Phys. Chem. A **111**, 8277 (2007).
[19] L. Cui and L. Wang, J. Phys. Chem. A **110**, 10169 (2006).
[20] L. Cui and L. Wang, Int. Rev. Phys. Chem. **27**, 139 (2008).
[21] Y. Negishi, H. Kawamata, A. Nakajima, and K. Kaya, J. Electron Spectrosc. **106**, 117 (2000).
[22] S. Furuse, K. Koyasu, J. Atobe, and A. Nakajima, J. Chem. Phys. **129**, 064311 (2008).
[23] W. A. de Heer, Rev. Mod. Phys. **65**, 611 (1993).
[24] P. C. Engelking, J. Chem. Phys. **87**, 936 (1987).
[25] C. Bréchignac, Ph. Cahuzac, J. Leygnier, and J. Weiner, J. Chem. Phys. **90**, 1492 (1989).
[26] M. F. Jarrold, U. Ray, J. E. Bower, and K. M. Creegan, J. Chem. Soc. Faraday Trans. **86**, 2537 (1990).
[27] W. Begemann, K. H. Meiwes-Broer, and H. O. Lutz, Phys. Rev. Lett. **56**, 2248 (1986).
[28] V. A. Spasov, T. H. Lee, and K. M. Ervin, J. Chem. Phys. **112**, 1713 (2000).
[29] C. Walther, S. Becker, G. Dietrich, H. J. Kluge, M. Lindinger, K. Lützenkirchen, L. Schweikhard, and J. Ziegler, Z. Phys. D **38**, 51 (1996).
[30] S. Krückeberg, L. Schweikhard, J. Ziegler, G. Dietrich, K. Lützenkirchen, and C. Walther, J. Chem. Phys. **114**, 2955 (2001).
[31] K. Hansen, Philos. Mag. B **79**, 1413 (1999).
[32] W. Bouwen, P. Thoen, F. Vanhoutte, S. Bouckaert, F. Despa, H. Weidele, R. E. Silverans, and P. Lievens, Rev. Sci. Instrum. **71**, 54 (2000).
[33] J. De Haeck, Ph.D. thesis, KU Leuven, 2011.
[34] E. Janssens, P. Gruene, G. Meijer, L. Wöste, P. Lievens, and A. Fielicke, Phys. Rev. Lett. **99**, 063401 (2007).
[35] S. M. Lang, P. Claes, N. T. Cuong, M. T. Nguyen, P. Lievens, and E. Janssens, J. Chem. Phys. **135**, 224305 (2011).
[36] P. R. Vlasak, D. J. Beussman, M. R. Davenport, and C. G. Enke, Rev. Sci. Instrum. **67**, 68 (1996).
[37] N. Veldeman, E. Janssens, K. Hansen, J. De Haeck, R. E. Silverans, and P. Lievens, Faraday Discuss. **138**, 147 (2008).
[38] C. Rajesh and C. Majumder, J. Chem. Phys. **126**, 244704 (2007).
[39] C. Bréchignac, H. Busch, Ph. Cahuzac, and J. Leygnier, J. Chem. Phys. **101**, 6992 (1994).
[40] S. Krückeberg, G. Dietrich, K. Lützenkirchen, L. Schweikhard, C. Walther, and J. Ziegler, Int. J. Mass. Spectrom. **155**, 141 (1996).
[41] K. Hansen and U. Näher, Phys. Rev. A **60**, 1240 (1999).
[42] Y. Saito, K. Yamauchi, K. Mihama, and T. Noda, Jpn. J. Appl. Phys. **21**, L396 (1982).
[43] G. F. Bertsch, N. Oberhofer, and S. Stringari, Z. Phys. D **20**, 123 (1991).
[44] S. Frauendorf, Z. Phys. D **35**, 191 (1995).
[45] P. Fröbrich, Phys. Lett. A **202**, 99 (1995).
[46] D. H. E. Gross and P. A. Hervieux, Z. Phys. D **35**, 27 (1995).
[47] W. Ashcroft and N. D. Mermin, in *Solid State Physics* (Holt Saunder, Tokyo, 1981), p. 461.
[48] K. Hansen and E. E. B. Campbell, Int. J. Mass. Spectrom. **233**, 215 (2004).
[49] H. Sontag and R. Weber, J. Mol. Spectrosc. **100**, 75 (1983).
[50] D. D. Stranz and R. K. Khanna, J. Chem. Phys. **74**, 2116 (1981).